Available online at www.sciencedirect.com
SCIENCE DIRECT®
Journal of Sound and Vibration 262 (2003) 475–496
JOURNAL OF SOUND AND VIBRATION
www.elsevier.com/locate/jsvi

A study of damping in fiber-reinforced composites

Rakesh Chandra[a], S.P. Singh[b,*], K. Gupta[c]

[a] *Dr. B.R.A. Regional Engineering College, Jalandhar, India*
[b] *Department of Mechanical Engineering, Indian Institute of Technology, New Delhi 110 016, India*
[c] *Indian Institute of Technology, Delhi 110 016, India*

Received 9 January 2002; accepted 13 January 2003

Abstract

Damping contributions from the viscoelastic matrix, interphase and the dissipation resulting from damage sites are considered to evaluate composite material damping coefficients in various loading modes. The paper presents the results of the FEM/Strain energy investigations carried out to predict anisotropic-damping matrix comprising of loss factors η_{11}, η_{22}, η_{12} and η_{23} considering the dissipation of energy due to fiber and matrix (two phase) and correlate the same with various micromechanical theories. Damping in three phase (i.e., fiber–interphase–matrix) composite is also calculated as an attempt to understand the effect of interphase. The contribution of energy dissipation due to sliding at the fiber–matrix interface is incorporated to evaluate its effect on η_{11}, η_{22}, η_{12} and η_{23} in fiber-reinforced composite having damage in the form of hairline debonding. Comparative studies of the various micromechanical theories/models with FEM/Strain energy method for the prediction of damping coefficients have shown consistency when both the effect of variable nature of stress and the fiber interaction is considered. Parametric damping studies for three phase composite have shown that the change in properties of fiber, matrix and interphase leads to a change in the magnitude of effectiveness of interphase, but the manner in which the interphase would affect the various loss factors depends predominately upon whether the hard or soft interphase is chosen. Analysis of the effect of damage on composite damping indicates that it is sensitive to its orientation and type of loading.

1. Introduction

Damping is an important parameter related to dynamic behavior of fiber-reinforced composite structures. The successful characterization of dynamic response of viscoelastically damped

*Corresponding author. Tel.: 91-11-26591136; fax: 91-11-26582053.
E-mail addresses: rakesh_iit@hotmail.com (R. Chandra), spsingh@mech.iitd.ernet.in (S.P. Singh), kgupta@mech.iitd.ernet.in (K. Gupta).

0022-460X/03/$ - see front matter © 2003 Published by Elsevier Science Ltd.
doi:10.1016/S0022-460X(03)00107-X

composite materials to prescribed modes of loading and time histories depends upon use of an appropriate analytical model/method, describing properties of composites based upon its constituents and their interaction, condition of interphase, presence of defects and selection of computational techniques. Composites are anisotropic and non-uniform bodies and a description of damping process in these materials calls for essential new development in the theory of damping. Zioniev and Ermakov [1] have classified the studies on composites as experimental investigations to generate damping data, the value and meaning of damping characteristics, their relation with material internal structure and development of damping theories/models in order to fully describe the energy dissipation process in composite materials. The mechanisms to which the dissipation energy can be attributed are: the viscoelastic nature of the matrix and/or fiber materials, damping due to interphase [2], damping due to damage [3], and viscoelastic damping at large amplitudes of vibration or high stress/strain levels and thermoelastic damping [4].

The effect of various damping mechanisms has been taken care of either individually or in combination, while modelling damping in fiber-reinforced composites. Chang and Bert [5], Crema and Castellani [6], Saravanos and Chamis [7,8], Kaliske and Rother [9], Chandra et al. [10,11] have predicted damping coefficients of fiber-reinforced composites considering the dissipation of energy due to fiber and matrix only whereby referring to it as a two-phase composite.

The contribution of three phases i.e., fiber–interphase–matrix in composites towards damping evaluation has been studied by Chaturvedi and Tzeng [12], Vantomme [13], Gibson et al. [2], Finegan and Gibson [14], and Chandra [15] and is incorporated in damping models. Further, the effect of damage is modelled by the finite element approach using a 2-D friction element. A pseudo dynamic approach is proposed to predict total loss factors of composites for different loadings for a single fiber–matrix debonding [15]. An integrated approach to study the effect of fiber–matrix, interphase and the dissipation resulting from damage sites at the fiber–matrix interface on the damping are considered here for fiber-reinforced composites. This has been achieved using FEM models developed for the two-phase composites and upgrading the same for the composite with interphase and damage.

2. Composite damping mechanisms

A detailed review of the damping studies in fiber-reinforced composites is given by Chandra et al. [16]. Different sources of energy dissipation in fiber-reinforced composites are briefly discussed below.

(1) Viscoelastic nature of matrix and/or fiber materials: the major contribution to composite damping is due to the matrix. However, fiber damping must be included in the analysis for carbon and Kevlar fibers, which have higher damping as compared to other types of fibers. Damping models, which consider the effect of dissipation of energy due to fiber and matrix in fiber-reinforced composite, are called two-phase models.

(2) Damping due to interphase: interphase [2] is the region adjacent to the fiber surface all along the fiber length. The interphase possesses a considerable thickness and its properties are different from those of embedded fiber and bulk matrix. The nature of interphase: weak, ideal or strong accordingly affects the mechanical properties and in turn damping of the fiber-reinforced

composites. Changing composite material comprised of fiber–interphase–matrix leads to modification of its overall damping.

(3) Damping due to damage: it is mainly of two types: (i) frictional damping due to slip in unbound regions between fiber and matrix interface or delaminations, and (ii) damping due to dissipation in the area of matrix cracks, broken fibers, etc.

Increase in damping due to fiber–matrix interfacial slip is reported to be significant [3]. Also, damping is more sensitive than stiffness to damage in a composite [17].

(4) Viscoelastic damping at large amplitudes of vibration or high stress/strain levels exhibits an evident degree of non-linear damping due to the presence of high stress and strain concentration in the local regions between fibers [4].

(5) Thermoplastic damping is due to cyclic heat flow from the region of compressive stress to the region of tensile stress in the composite, especially in thermoplastic composites [18].

Damping studies considering the composite as two-phase or three-phase systems and modelling of damage at the fiber matrix interface for damping is reported as an integrated approach in this paper.

3. Analysis for damping

Micromechanical damping analysis of unidirectional fiber-reinforced composites involves the determination of contribution of its constituents, i.e., fiber, matrix, interphase and condition of the fiber–matrix interface. In this paper, initially it is presumed that there is perfect bonding between fiber and matrix, and the composite is considered to be made up of two phases (fiber–matrix). The concept developed for a two-phase model is extended to three-phase composites (fiber–interphase–matrix). Further, the effect of the condition of fiber–matrix interface, i.e., damage (micro-crack) or discontinuity at the fiber–matrix interface is incorporated in the two-phase composites.

3.1. Two- and three-phase damping models

The strain energy method proposed by Ungar and Kerwin [19] expresses, for a given loading, the composite loss factor as the ratio of the summation over all elements of the structure of the product of the loss factor for each element and the strain energy for each element to the total strain energy.

Thus the loss factor for the three-phase model considering the effect of fiber, matrix and interphase can be expressed as

$$\eta = \frac{\sum_{i=1}^{n} \eta_i W_i}{\sum_{i=1}^{n} W_i}, \tag{1}$$

$$\eta_c = \frac{(\eta_f W_f + \eta_m W_m + \eta_i W_i)}{W_c}. \tag{2}$$

The strain energy stored in the composite under loading can be written as

$$W_c = \tfrac{1}{2}\int_V \sigma_{ij}\varepsilon_{ij}\,\mathrm{d}V = \tfrac{1}{2}\sum \sigma_{ij}\varepsilon_{ij}\,\delta V = \tfrac{1}{2}\sum \sigma_{ij}^{\mathrm{T}} S_{ij}\sigma_{ij}\delta V. \tag{3}$$

The total strain energy of composite can also be expressed as the sum of the contributions from its constituents, i.e., fiber, matrix and interphase respectively,

$$W_c = (W_f + W_m + W_i). \tag{4}$$

The strain energy stored in the constituents, i.e., fiber matrix and interphase in a unit cell of a certain volume is given as

$$W_f = \tfrac{1}{2}\sum \{\sigma_{ij}\}_f^{\mathrm{T}}\{S_{ij}\}_f\{\sigma_{ij}\}_f\delta V_f, \tag{5}$$

$$W_m = \tfrac{1}{2}\sum \{\sigma_{ij}\}_m^{\mathrm{T}}\{S_{ij}\}_m\{\sigma_{ij}\}_m\delta V_m, \tag{6}$$

$$W_i = \tfrac{1}{2}\sum \{\sigma_{ij}\}_i^{\mathrm{T}}\{S_{ij}\}_i\{\sigma_{ij}\}_i\delta V_i. \tag{7}$$

The above relationships can be modified for two-phase composite by ignoring the contribution of the interphase due to its absence, i.e., $W_i = 0$ and $\eta_i = 0$. The above formulation is adopted for FEM modelling of loss factors in composite materials. Some of the important research papers of Gibson et al. [2] and Finegan and Gibson [14] made use of a FEM/Strain energy approach to predict damping in fiber-reinforced composites.

3.2. Modelling for interface damage

Damage in glass fiber-reinforced epoxy considered here is represented by a hairline crack with zero gap width at the fiber–matrix interface. Any discontinuity in the composite is referred as geometrical non-linearity. This discontinuity at the fiber–matrix interface is modelled by application of a non-linear gap element. Thus, the FEM modelling of interfacial discontinuity is considered as non-linear. The gap element facilitates modelling of a discontinuity at the interface without or with the consideration of friction, respectively. As under dynamic loading, the fiber–matrix interface is bound to dissipate energy at the debonded region, it is appropriate to use friction elements to simulate the actual conditions. Further, in order to predict dissipation of energy per cycle, the non-linear/FEM model is subjected to static loads in steps varying from zero to maximum and to zero for a half load cycle during which the crack is in a closed condition. Hence, it is through the analysis of the set of static/non-linear FEM models that energy dissipation at the fiber–matrix interface is predicted.

A 2-D gap/friction element, which is a two noded non-linear element, provides node-to-node contact between the two bodies. The friction element is based on the law of friction relating the tangential (F_t) and normal (F_n) forces through a coefficient of friction (μ). In order to predict the dissipation of energy for one cycle due to sliding at the fiber–matrix interface caused by discontinuity (damage), the FEM model with an interface friction element is simulated for dynamic steady state loading. For this purpose, a sinusoidally varying load is applied to the composite. At various stages of the load the state of the composite is analyzed with respect to the forces and displacements in the damage region. The force–displacement variation over a complete cycle of loading is used to calculate the energy dissipated in the gap element. This approach is

pseudo-dynamic in nature since inertia effects are not considered and the dynamic loading is assumed as a series of static forces varying in a sinusoidal manner. Thus the force applied, F_i, varies as given in Eq. (8). A static non-linear FEM analysis is conducted for a number of discrete values of this force:

$$F_i = F_0 \text{ Sin } \omega t = F_0 \text{ Sin } \theta. \tag{8}$$

In the process of dynamic simulation, it is necessary to select the direction and magnitude of the excitation load for the static non-linear analysis. Here, non-linearity is introduced due to the geometric discontinuity, i.e., debonding at the fiber–matrix interface. The magnitude of amplitude F_0 is decided on the basis of linear elastic behavior of the glass fiber-reinforced composite (GFRE) for which the damping studies are under consideration. The excitation load for the corresponding static non-linear FEM models simulating the dynamic behavior under particular loading condition is increased gradually, starting from zero in a step increment of a certain fixed percentage of F_0.

In the process of performing a sensitivity analysis of the frictional element, it is observed that the gap remains in closed status for half of the loading cycle, while for the remaining half it attains an open status [15]. The dissipation of energy due to relative sliding at the fiber–matrix interface naturally occurs during the closed status of the discontinuity when the gap is in a sliding mode depending upon the instantaneous direction of the step load. Hence, for each type of loading, i.e., transverse, transverse shear, extensional and in-plane shear, it is important to select the direction of the load vector so that the relative sliding occurs between the nodes of the friction element belonging to fiber and matrix during a particular step load. The pseudo-dynamic approach is proposed to predict the contribution of energy dissipation due to sliding at the fiber–matrix interface. The steady state response of the FEM model is simulated by the application of load steps lying on a sinusoidal quarter cycle such that $0 \leqslant F_i \leqslant F_0$, where F_i is step load and F_0 is amplitude of the steady state load. Dissipation of energy due to the discontinuity at the interface is obtained by varying the step load from 0 to F_0 and then to 0 for half the cycle or for the quarter cycle with a step load from 0 to F_0 and analyzing the respective FEM models.

The output of the static non-linear FEM analysis for each load step provides F_t and the relative displacement d_s between the nodes of the friction element simulating the discontinuity at the interface. The area under the curve plotted between F_t vs d_s gives the dissipation of energy due to the interface for the quarter cycle. Thus, the energy dissipated per cycle at the interface due to the discontinuity is given by

$$D = 2 \times (\tfrac{1}{2} \times F_t \times d_s). \tag{9}$$

The total loss factor of the composite can be determined as the ratio of total energy dissipated and the maximum strain energy per cycle as

$$\eta_{total} = \frac{(D_f + D_m) + \sum_{j=1}^{n} (D_{id})_j}{W_{id}}. \tag{10}$$

Here j = index of friction element, n being their total number, D_f and D_m = energy dissipated by fiber and matrix, respectively, D_{id} = energy dissipation due to individual discontinuity at the interface, and W_{id} = total strain energy with interfacial discontinuity.

The contribution of the fiber–matrix can be expressed in terms of the loss factor and strain energy without consideration of fiber–matrix interface friction ($\mu = 0$) as

$$(D_f + D_m) = \eta_{wf} W_{id}, \tag{11}$$

where η_{wf} = loss factor without the consideration of friction at the interface.

Thus, Eq. (10) can be rewritten as

$$\eta_{total} = (\eta_{wf}) + \frac{\sum_{j=1}^{n} (D_{id})_j}{W_{id}}. \tag{12}$$

3.3. FEM modelling

FEM models for GFRE with various fiber volume fractions are constructed and subjected to different types of loading conditions. 2-D, 3-D static and 2-D static non-linear (with gap/friction element) FEM models are analyzed for the prediction of loss factors (η_{11}, η_{22}, η_{12} and η_{23}) for two- and three-phase models of composites with damage, respectively.

3.3.1. Two- and three-phase FEM modelling

The 2-D single-cell representative volume element (RVE) discretized by plane strain/plane stress elements is shown in Fig. 1. In addition to the lay out of the fiber and matrix elements, Fig. 1 also shows the boundary conditions for the respective type of loading for two-phase models. In case of transverse and transverse shear loading, the nodal points at the lower edge of the RVE are fixed by restricting all the degrees of freedom. For the longitudinal shear case the half-domain model is utilized. For the case of the longitudinal loading, constraints along the x-axis allows motion along the x-axis and restricts all other, whereas along the y-axis it restricts all except along the y-axis. For longitudinal shear, nodal constraints on the lower edge of the RVE restrict all the degrees of

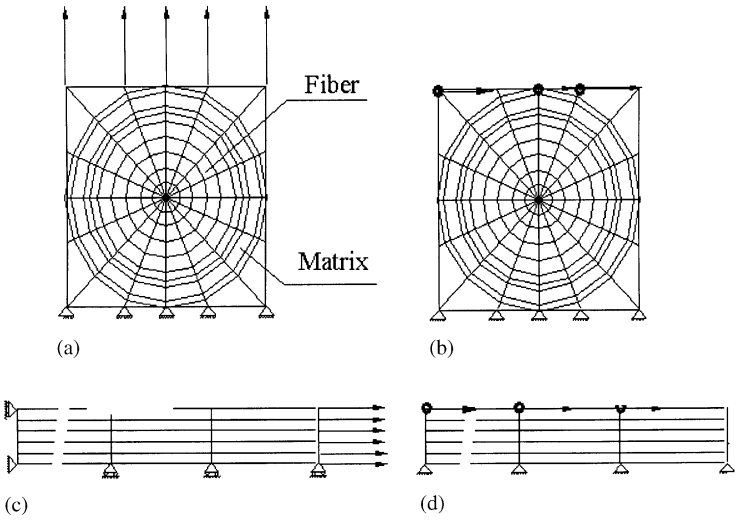

Fig. 1. FEM models for different loading conditions: (a) transverse, (b) transverse shear, (c) longitudinal, (d) longitudinal shear.

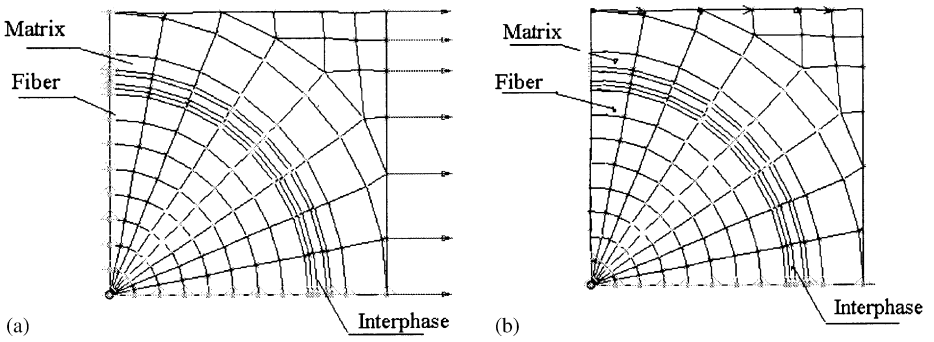

Fig. 2. 2-D FEM models with interphase for $V_f = 0.4$ (fixed), $V_i = 0.1$, $V_m = 0.5$, number of elements $N_f = 1-64$, $N_i = 65-96$, and $N_m = 97-130$. Loading conditions: (a) transverse and (b) transverse shear.

Table 1
Basic properties of GFRE constituents

Properties	E-glass fiber	Epoxy matrix	Hard-interphase	Soft-interphase
E (Gpa)	72.4	2.76	37.58	0.5
G (Gpa)	30.2	1.02	15.61	0.178
v	0.2	0.35	0.204	0.4
η	0.0018	0.015	0.0084	0.0084

freedom. Transverse uniform stress is applied at nodal points along the y-axis (Fig. 1(a)), whereas transverse shear acts on the face of the elements (Fig. 1(b)). Similarly, the nodal longitudinal stress is applied at the nodes perpendicular to the face of the respective element (Fig. 1(c)) for the case of the longitudinal model while longitudinal shear stress acts on the face of the elements (Fig. 1(d)) in case of longitudinal shear models, respectively. The analysis of the FEM models was performed for the prediction of the state of stress in the constituents of the composite. The strain energy stored in the fiber and matrix, and the loss factors for different loading conditions are obtained based on Eqs. (4)–(7). Strain energy is determined in the present study over the area of each element assuming a unit constant thickness. These two-phase FEM models have been modified by introducing an interphase between fiber and the matrix to predict its effect on composite damping.

2-D FEM models with interphase volume fraction $V_i = 0.02$, 0.04, 0.08 and 0.1 for transverse and transverse shear loading with single-cell square array packing are analyzed. Fig. 2(a) and (b) show the 2-D FEM model for transverse and transverse shear loadings, respectively. These models are constructed for a fixed fiber volume fraction $V_f = 0.4$ considering the interphase to be (1) hard: interphase properties are taken as average of the elastic properties of fiber and matrix; or (2) soft: interphase properties are lower than those of the matrix (see Table 1). This assumption is made because a precise estimation of the properties of the interphase is not available in the reported literature [12–13]. Similarly, the loss factor for both the soft and hard interphase is assumed to be the average of the loss factor of fiber and matrix, because no theoretical or experimental data is available in literature. Chaturvedi and Tzeng [12] assumed the loss factor of the interphase to be equal to that of the matrix because of a lack of information in this regard. Loss factors in

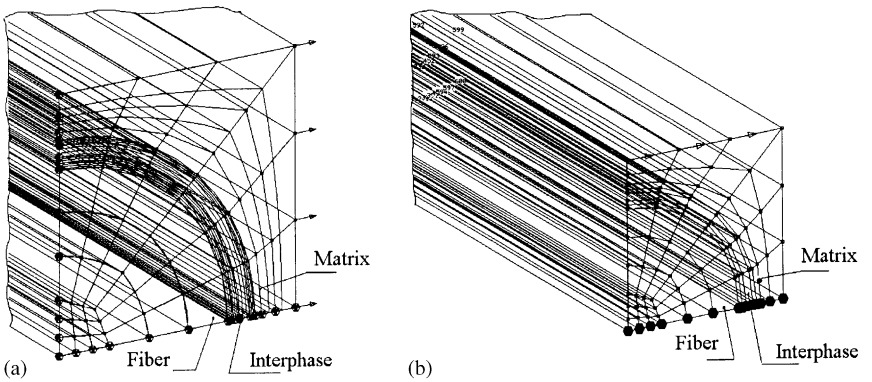

Fig. 3. 3-D FEM model for composite with interphase: $V_f = 0.4$ (fixed), $V_i = 0.1$, number of elements $N_f = 1-270$, $N_i = 271-510$, and $N_m = 511-690$. Loading conditions: (a) transverse, and (b) transverse shear.

transverse and transverse shear, longitudinal and longitudinal shear modes are also predicted using 3-D FEM models. 3-D FEM models with an interphase for transverse and transverse shear loading are shown in Fig. 3. Hexahedra eight noded elements are used to construct the FEM model for the fiber-reinforced composite with a fiber volume fraction $V_f = 0.4$ [15].

The total thickness of the interphase (T_i) is worked out such that the maximum value of $V_i = 0.1$ is further subdivided into a number of layers to obtain $V_i = 0.02$, 0.04, 0.08. A finer mesh size is used in the interphase near the fiber as well as near the matrix in order to correctly predict stresses in interphase region. Both a soft and a hard interphase is incorporated in the FEM models. The output of the static analysis of these FEM models is obtained in the form of the strain energy for the finite elements of fiber, matrix and interphase in the respective mode of loading. The strain energy of the constituent elements is determined using Eqs. (4)–(7) and corresponding loss factors (η_{11}, η_{22}, η_{12} and η_{23}) are predicted.

3.3.2. *FEM modelling for damage*

The interfacial discontinuity is modelled by single- and multiple-gap elements in case of transverse and transverse shear loading to study the effect of orientation as well as the effect of the number of gap elements for the same gap size. The orientation of gap θ_g is defined as angle subtended by the direction of the gap at the coincident nodes with respect to the global x-axis. The gap size θ_{gs} is referred as the included angle between the extreme merged nodes corresponding to beginning and end of the discontinuity. Thus the discontinuity is characterized by parameters: gap width (GW), gap size (θ_{gs}) number of gap elements and gap orientation (θ_g). In case of the single-gap element model, the orientation of gap coincides with the axis of symmetry of the gap, whereas for the multiple gap element model, an average gap orientation is considered which again refers to the axis of the symmetry of the gap. Single-gap element refers to use of only one friction element between a debonded fiber and the matrix interface. The three-gap element FEM model incorporates, for the same gap size, three friction elements.

A representative FEM model for transverse loading with a single-gap element having $\theta_g = 45^\circ$ and $\theta_{gs} = 45^\circ$ is shown in Fig. 4(a). It consists of 80 quadrilateral four noded elements comprised of a number of elements in the fiber (N_f) from 1 to 48, and elements in the matrix (N_m) from 49 to 80,

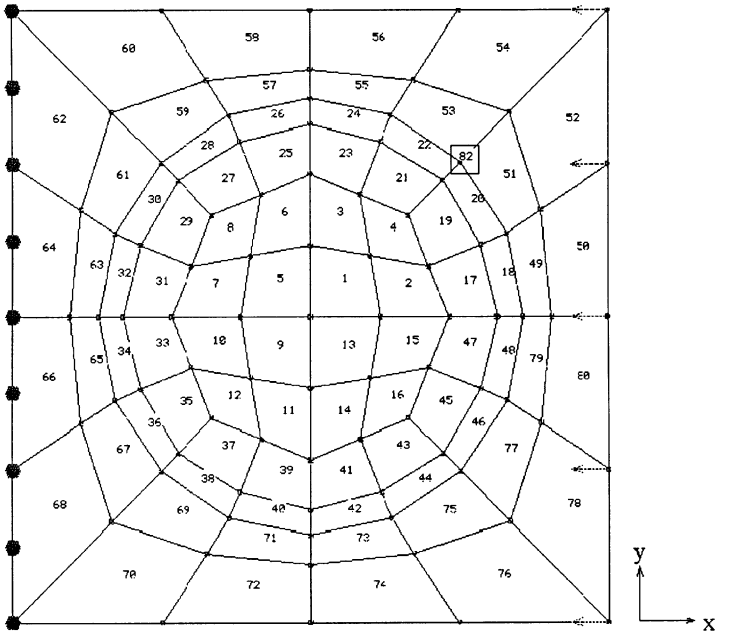

(a)

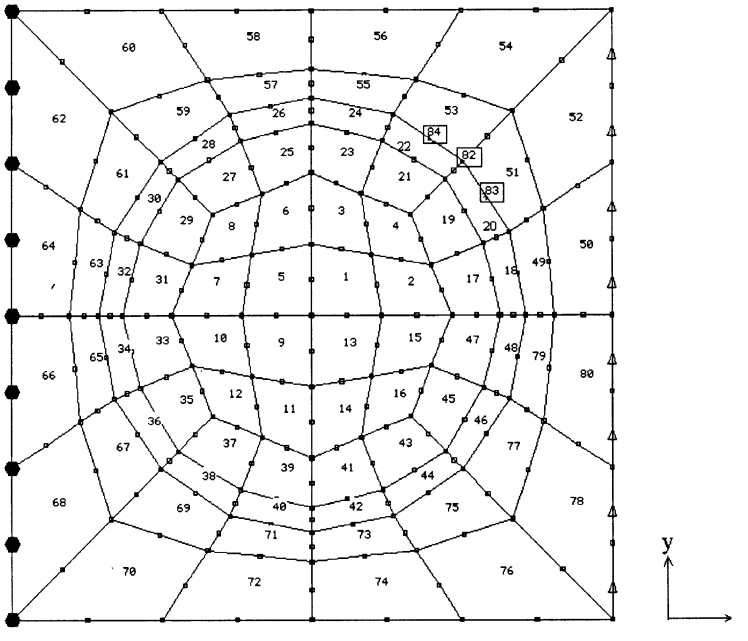

(b)

Fig. 4. Static/non-linear FEM model for (a) transverse loading with a single-gap element, $N_g = 82$, and (b) transverse shear loading with three-gap elements, $N_g = 82-84$. Model: $V_f = 0.4$, number of elements $N_f = 1-48$.

in addition to one friction element, $N_g = 82$. The model is analyzed for several load steps F_i which is increased gradually from 0 to 1N in an increment of 0.1 such that $0 \leqslant F_0 \leqslant F_i$. The corresponding output F_t, d_s, W_f and W_m is recorded.

Various static non-linear FEM models, also with a single-gap element for different gap orientations, θ_g varying from 0 to 180° in step of 22.5°, are analyzed in combination with a pseudo dynamic approach to obtain strain energy of the constituent finite element and the energy dissipated at the interface due to debonding in different loading conditions. Fig. 4(a) also elaborates how the single-gap element is incorporated in the various FEM models to study the effect of gap orientation on overall damping. The gap orientation varies from 0 to 180° in a step of 22.5°, which refers to the direction of discontinuity at the fiber matrix interface. Three-gap element FEM models for transverse loading are obtained by replacing single-gap elements by three-gap elements. The purpose of using three-gap elements is to study the effect of the number of friction (gap) elements on the dissipation of energy at the interface for the same gap size (θ_{gs}). So three friction elements are introduced along the fiber–matrix interface for the same gap size ($\theta_{gs} = 45°$) as in case of single-gap element models. The orientation of three friction elements within the gap can be seen from Fig. 4(b): θ_g with respect to the global x-axis is 45° (position of friction element number $N_g = 82$) and $\theta_i = \pm 11.25°$ with respect to the gap axis (position of friction element $N_g = 84$ and 83). Fig. 4(b) shows the static non-linear FEM model with the application of three-gap elements. Models with three-gap elements for different gap orientations, $\theta_g = 0$ to 180° in steps of 22.5°, are analyzed for the non-linear static case and are drawn for all gap elements maintaining closed status for all step loads ($0 \leqslant F_i \leqslant F_0$). Energy dissipated due to slip at the interface in transverse loading for single and three-gap element models are predicted [15]. Representative $F_t - d_s$ plots (for $\theta_g = 0$–180°) for static/non-linear FEM models with three-gap elements under transverse loading are given in Fig. 5. Each area under these curves can be evaluated to obtain the individual contribution of gap elements to the total dissipated energy due to the gap size $\theta_{gs} = 45°$.

A pseudo-dynamic approach is used to predict total loss factor of composite for various orientations of gap element. In this approach, the following procedure is adopted for all the damping predictions for models with friction elements.

Step 1: determine the loss factor for the composite when $\mu = 0$ using Eq. (11).

Step 2: plot a graph between F_t and d_s for the corresponding incremental loads for $0 \leqslant F_0 \leqslant F_i$. The area under the $F_t - d_s$ curve provides the energy dissipated for the quarter cycle of the steady state load, $F_t = F_0 \operatorname{Sin} \omega t$.

Step 3: use Eq. (12) to predict the total loss factor η_{22}, considering dissipation of energy due to fiber, matrix and due to sliding at the interface, i.e., friction.

The percentage increase in loss factor due to interface sliding, with respect to a pristine material loss factor is expressed under transverse loading as

$$\% \text{ increase in loss factor } \eta_{22} = \frac{(\eta_{22})_t - (\eta_{22})_p}{(\eta_{22})_p} \times 100. \tag{13}$$

In a similar way FEM models with single/three-gap elements for the transverse shear loading condition and relevant boundary conditions are analyzed in order to predict the total shear loss factor $(\eta_{23})_t$ and the percentage increase in $(\eta_{23})_t$ for the respective case.

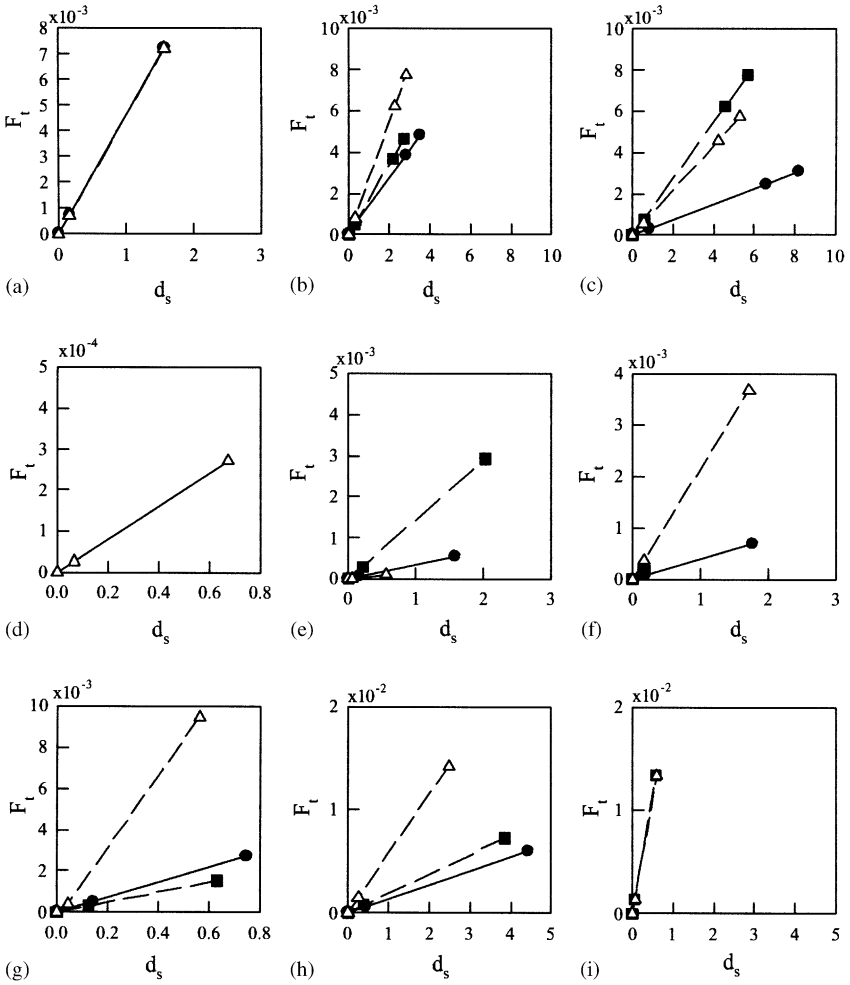

Fig. 5. Energy dissipated at the interface due to friction: transverse loading, three-gap element model (gap element ●, GE-82; ■, GE-83; and △, GE-84) for orientation of gap axis θ_g (a) 0°, (b) 22.5°, (c) 45°, (d) 67.5°, (e) 90°, (f) 112.5°, (g) 135°, (h)157.5°, and (i) 180°.

Discontinuity at the fiber–matrix interface, in case of longitudinal and longitudinal shear is considered to be around the circumference of the fiber. Due to symmetry, a 2-D half-domain FEM model is used, and the discontinuity is modelled by a single-gap element. The position of discontinuity is identified along the fiber axis by the location of the gap element, and defined as the ratio x/l (Fig. 6). Here, x is the location of gap element with respect to the left edge of the model and l is the length of the model along the fiber axis. Longitudinal or longitudinal shear loading is applied, while analyzing the corresponding model.

Typical 2-D FEM models with single-gap element for longitudinal and longitudinal shear loading with a discontinuity starting at the extreme right hand side and showing the loading and boundary conditions are depicted in Fig. 6. Each model consists of eight noded quadrilateral

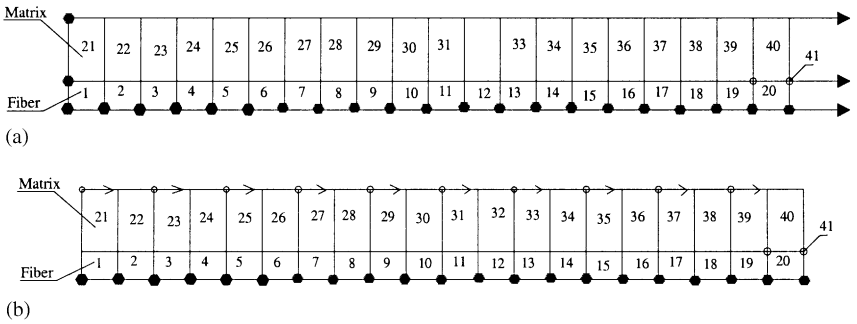

Fig. 6. Static/non-linear FEM model with single-gap element for different loadings model; $V_f = 0.4$, number of elements in fiber $N_f = 1 - 20$, in matrix $N_m = 21 - 40$ and gap element $N_g = 41$. (a) Longitudinal loading, (b) shear loading.

elements: 1 to 20 in the fiber and 21-40 in the matrix. Element number 41 is a gap element at the location $x/l = 1$.

The total loss factor in extension and shear is predicted using Eqs. (11) and (12). In Eq. (12) the respective loss factors are replaced by ones corresponding to the respective loading condition.

4. Results and discussions

The total loss factor for a composite is due to the contributions of fiber, matrix and energy dissipated because of sliding at the damaged interface. Results of damping predictions based on the integrated FEM/Strain energy approach considering the above-mentioned mechanisms are presented here.

4.1. Two-phase composite

Damping coefficients predicted by FEM/strain energy modelling and from various other micromechanical models [7, 20–25] for two-phase composites are presented in Table 2 for a fiber volume fraction of 0.4. Table 2 shows that for the given fiber volume fraction the FEM/strain energy prediction for η_{11} compares well with those of the Saravanos–Chamis approach, and the

Table 2
Comparison of loss moduli using various models/methods

Model/method	η_{11}	η_{22}	η_{12}	η_{23}
Eshelby	9.867×10^{-4}	1.40593×10^{-2}	1.41181×10^{-2}	1.43321×10^{-2}
Tsai	—	1.42107×10^{-2}	1.41×10^{-2}	—
Hashin	2.514×10^{-3}	1.433×10^{-2}	1.41×10^{-2}	—
Halpin–Tsai	—	1.358×10^{-2}	1.4118×10^{-2}	—
FEM/Strain energy	2.6539×10^{-3}	1.4495×10^{-2}	1.4712×10^{-2}	1.4489×10^{-2}
Saravanos–Chamis	2.514×10^{-3}	1.10159×10^{-2}	1.10159×10^{-2}	1.0544×10^{-2}

Hashin model also indicates that the predictions made by Eshelby's method are not accurate enough. Loss factors η_{22}, η_{12} and η_{23} predicted by the FEM/strain energy method correlate very well. A detailed comparative study of damping predictions by the FEM/strain energy method in reference to other models/methods has been studied by the authors and reported previously [25].

4.2. Three-phase composites

Loss factors η_{11}, η_{22}, η_{23}, and η_{12} are evaluated for fixed fiber volume fraction ($V_f = 0.4$) by changing the interphase volume fraction between the ranges of 0.02–0.1 for a low interphase loss factor of the order of 0.0084. Fig. 7 shows variation of loss factors η_{11}, η_{22}, η_{23}, and η_{12} as function of interphase volume fraction (for both soft and hard interphase) using the FEM/Strain energy method. The loss factor η_{11} is almost constant in case of a composite with a soft interphase, whereas there is some increase when the hard interphase is incorporated. Curve 3 indicates that there is decrease in loss factor η_{22} as the interphase volume fraction increases in the composite with soft interphase. In contrast, the presence of a hard interphase does not have any effect on η_{22} with the increase in V_i. Similar behavior is observed for the loss factor of a composite with soft and hard interphase, respectively. Loss factor η_{12} of a three-phase composite is predominantly

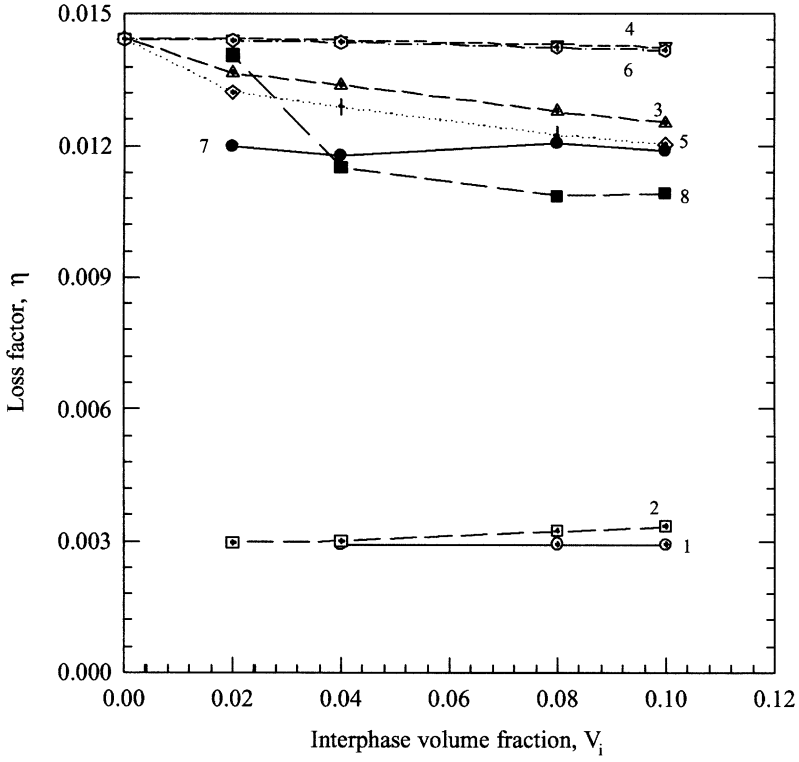

Fig. 7. Effect of interphase volume fraction on loss factor 1–η_{11} (soft interphase), —⊙—; 2–η_{11} (hard interphase), - -⊡- -; 3–η_{22} (soft interphase), - -△- -; 4–η_{22} (hard interphase), - -▽- -; 5–η_{12} (soft interphase), ····◇····; 6–η_{12} (hard interphase), - -⊙- -; 7–η_{23} (soft interphase), —●—; 8–η_{23} (hard interphase),- -■- -.

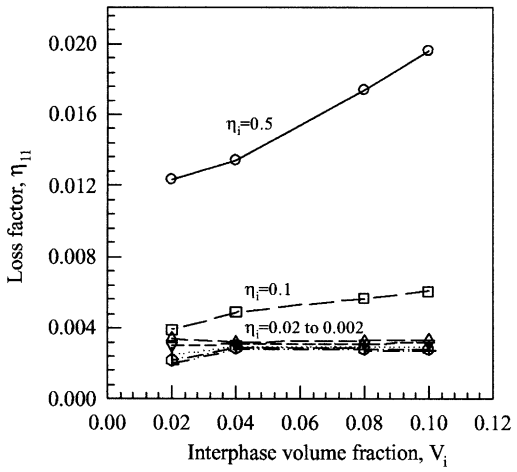

Fig. 8. Variation of loss factor η_{11} as a function of V_i (3-D FEM model with soft interphase).

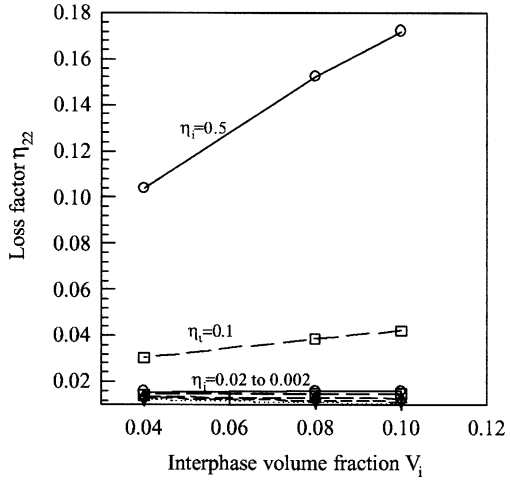

Fig. 9. Variation of loss factor η_{22} as a function of V_i (3-D FEM model with soft interphase).

dependent upon the status of the interphase, which is clear from curves 6–7. It is observed that η_{12} for a composite with a soft interphase decreases appreciably with increase in V_i as compared to the case of a hard interphase. A marginal reduction in η_{12} with a hard interphase is due to minor variation in the strain energy component of the interfacial region. It may be noted that the over all loss factor of composite from the FEM model is dependent on assumed values of interphase properties, i.e., loss factor and elastic modulus. A gradual decrease in the value of η_{23} is predicted with increasing V_i in case of a composite with a hard interphase (curve 8) whereas there is very minor change in its value in case of a soft interphase (curve 7). Further details concerning the percentage contribution of individual constituents, i.e., fiber, matrix and interphase, to the overall loss factor of the fiber-reinforced composite are given by Chandra et al. [26].

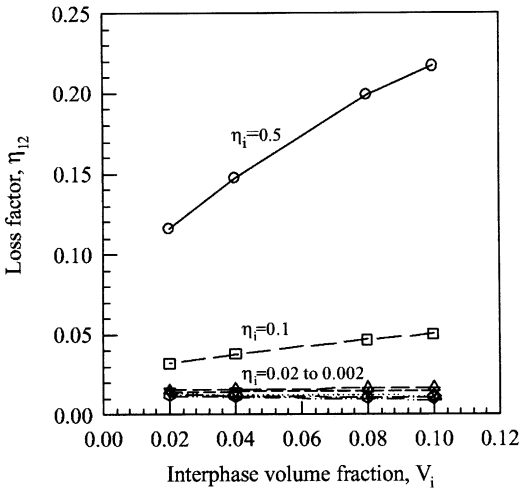

Fig. 10. Variation of loss factor η_{12} as a function of V_i (3-D FEM model with soft interphase).

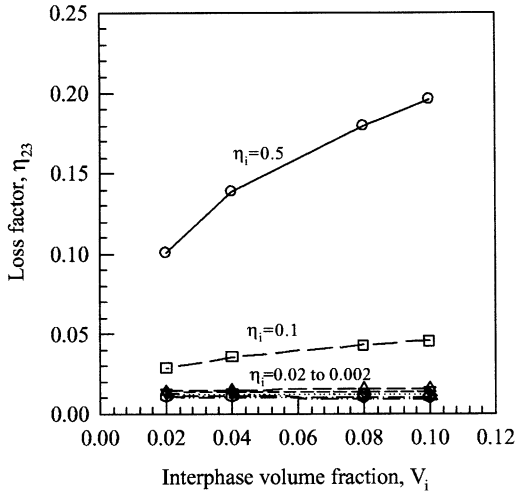

Fig. 11. Variation of loss factor η_{23} as a function of V_i (3-D FEM model with soft interphase).

A parametric study of the interphase is shown in Figs. 8–11. The effect of variation of interphase loss factor for different interphase volume fraction on the composite loss factor is shown in Figs. 8–11. It can be seen that the interphase loss factor for higher values (0.1–0.5) has a predominant effect on the composite loss factor under all loadings, i.e., longitudinal, transverse, longitudinal shear and transverse shear. Higher values of the η_i loss factors show faster increasing damping trend with increase in interphase volume fraction. At lower values of interphase damping η_i, the composite loss factors for all loadings show very little variation.

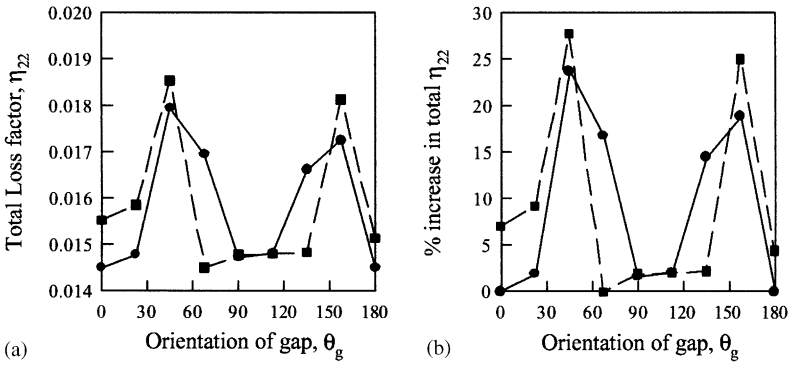

Fig. 12. Effect of number of gap elements on: (a) total η_{22}, (b) percentage increase in total η_{22} (FEM model: gap size $\theta_{gs}=45^\circ$; $V_f=0.4$; ●, single-gap element; ■, three-gap element).

Table 3
Variation of d_s and F_t with gap orientation θ_g

Gap orientation θ_g	Sliding distance d_s (μm)	$F_t \times 10^{-2}$ (N)
0	0	0
22.5	0.64716	1.064379
45	8.8003	0.9783104
67.5	8.3086	0.7336094
90	4.0153	0.298794
112.5	2.8348	0.2666007
135	6.0597	0.865095
157.5	4.1404	1.636684
180	0	0

4.3. *Effect of interface damage*

Results pertaining to the total transverse loss factor η_{22} obtained from single- and three-gap element models are discussed first. Energy dissipated at the interface for three-gap element models can be obtained from Fig. 5 by adding contributions of individual gap elements. In accordance with the basic principal underlying the interface element [27], here tangential force, F_t varies linearly with respect to relative sliding between the coincident nodes belonging to fiber and matrix at the interface in contact. As the gap remains closed for half the cycle, the dissipation of energy is given by Eq. (9). Similar behavior is observed for single-gap element models. Variation of $(\eta_{22})_t$ and the percentage increase in $(\eta_{22})_t$ with respect to θ_g for a single-gap FEM model is shown in Fig. 12(a) and (b), respectively. Fig. 12(a) shows that an appreciable increase in damping takes place as the orientation of the gap (and the angle with respect to the direction of load vector) changes from 0 to 45°. The reason is that the relative sliding distance (d_s) increases with an increase in θ_g, although there is a decrease in F_t. For the gap orientation $\theta_g=0^\circ$, $D_i=0$, and therefore $(\eta_{22})_t$ reduces to $(\eta_{22})_{wf}$. Moreover, $F_t=0$, and for such a situation, the normal force F_n is very high, leading to a close status of the gap with a sticking mode. As θ_g equals 22.5°, the angle

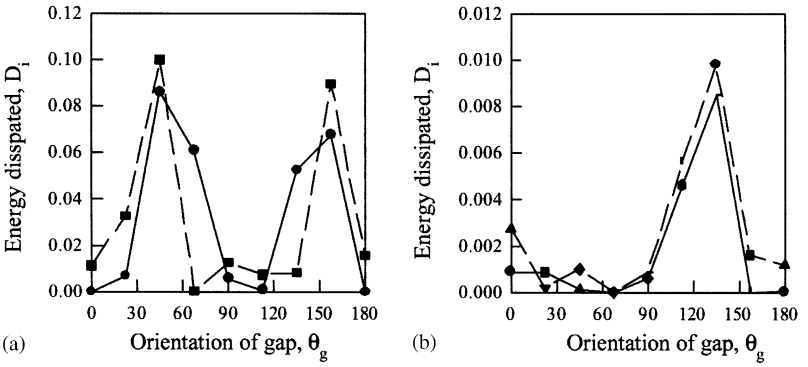

Fig. 13. Variation of energy dissipated by gap under (a) transverse, (b) transverse shear loading (FEM model: gap size $\theta_{gs}=45^\circ$; $V_f=0.4$; —●—, single-gap element; —■—, three-gap element).

between the average load vector and the gap direction becomes 22.5°. Table 3 shows the sliding distance (d_s) and F_t, for different values of θ_g, which have a direct bearing on the value of D_i. It can be seen that although F_t decreases marginally with θ_g, the magnitude of d_s increases, leading to larger dissipation of energy at the interface. This is true up to $\theta_g=45^\circ$. Further, for $45^\circ \leqslant \theta_g \leqslant 90^\circ$, there is a continuous decrease in F_t and d_s. The following ratio gives a quantitative idea; for example, $(F_t)_{\theta=67.5^\circ}/(F_t)_{\theta=45^\circ}=0.75$ and $(F_t)_{\theta=90^\circ}/(F_t)_{\theta=45^\circ}=0.30$, whereas $(d_s)_{\theta=67.5^\circ}/(d_s)_{\theta=45^\circ}=0.94$ and $(d_s)_{\theta=90^\circ}/(d_s)_{\theta=45^\circ}=0.46$. Thus, under the combined effects of F_t and (d_s), $(\eta_{22})_t$ decreases for $45^\circ \leqslant \theta_g \leqslant 90^\circ$.

There is a slight increase in $(\eta_{22})_t$ for $\theta_g=112.5^\circ$. Thereafter, similar behavior for $(\eta_{22})_t$ is repeated for $112.5^\circ \leqslant \theta_g \leqslant 180^\circ$ with a maximum at $\theta_g=157.5^\circ$. Once again at $\theta_g=180^\circ$, direction of load vector and gap direction coincide, leading to $D_{i=}0$ and thus reducing to $(\eta_{22})_t=(\eta_{22})_{wf}$. The variation of D_i vs θ_g for single-gap element models is shown in Fig. 13(a). A sharp increase in the value of D_i is clearly seen for θ_g in the region of about 45° and 157.5°, which explains the fact that $(\eta_{22})_t$ attains the peak values at these angles. Fig. 12(b) shows the percentage increase in $(\eta_{22})_t$ as a function of θ_g. Its pattern of variation is exactly similar to $(\eta_{22})_t$. It has an increasing trend for $0^\circ \leqslant \theta_g \leqslant 45^\circ$, followed by a reducing trend for $45^\circ \leqslant \theta_g \leqslant 67.5^\circ$. An increasing trend is again observed for $112.5^\circ \leqslant \theta_g \leqslant 157.5^\circ$. Similar behavior is observed for $180^\circ \leqslant \theta_g \leqslant 360^\circ$ (the results are not presented here) due to the geometric symmetry of the model.

Figs. 12(a) and (b) also show $(\eta_{22})_t$ and the percentage increase in $(\eta_{22})_t$ for models with three-gap elements with respect to θ_g. The behavior of $(\eta_{22})_t$ and % increase in $(\eta_{22})_t$ is similar to the one for models with a single-gap element. This is also clear from the comparison of energy dissipated per cycle for the two types of models in transverse loading as shown in Fig. 13(a). The reason for higher D_i, say for $\theta_g=0^\circ$, is due to the contribution of gap elements having a gap orientation $\theta_g=\pm 11.25^\circ$ with respect to the gap axis. Similarly, Figs. 12(a) and (b) show that the peak value of $(\eta_{22})_t$ and the percentage increase in $(\eta_{22})_t$ correspond to $\theta_g=45^\circ$ and 157.5° as in case of single-gap element models. However, their magnitudes are on the higher side. The percentage increase in $(\eta_{22})_t$ for a single-gap element is 23.75 whereas for the three-gap element model, it is 27.8 at $\theta_g=45^\circ$. Corresponding to the other peak, i.e., at $\theta_g=157.5^\circ$, the value of the percentage increase in $(\eta_{22})_t$ is 18.85 and 25.08, respectively, for the single-gap element and three-gap element models.

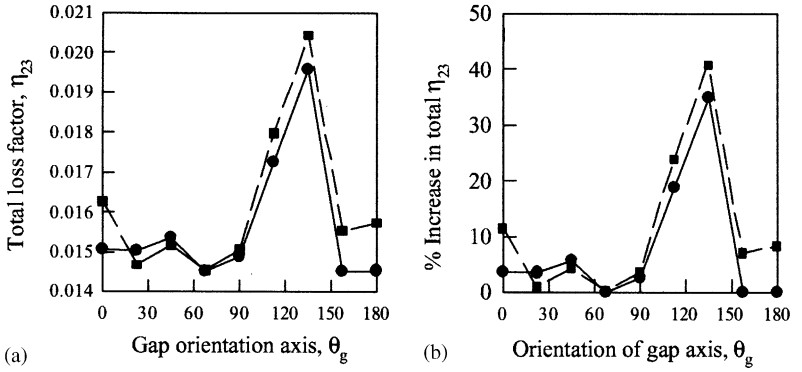

Fig. 14. Effect of number of gap elements on: (a) total η_{23}, (b) percentage increase in total η_{22} (FEM model: gap size $\theta_{gs}=45^\circ$; $V_f=0.4$; •, single-gap element; ■, three-gap element).

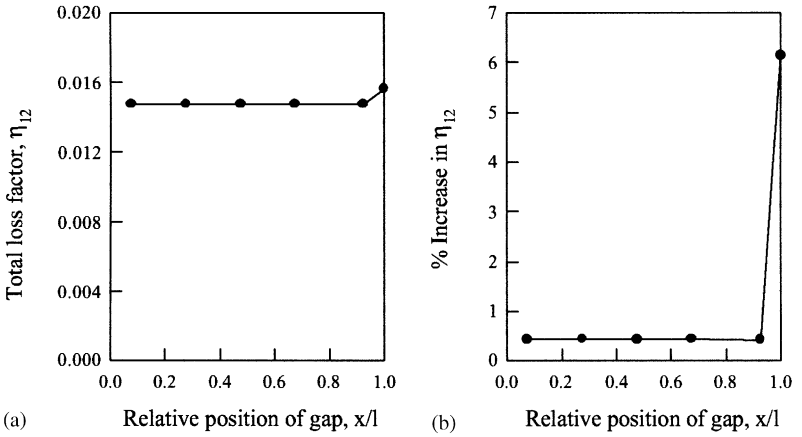

Fig. 15. Effect of location of gap on (a) total η_{12} and (b) percentage increase in total η_{12} (FEM model: inplane shear loading; no. of gap elements = 1; gap size = 23.76 μm; $V_f=0.4$).

The comparison of the results shows a marginal difference in value of percentage increase in $(\eta_{22})_t$ for $\theta_g=45^\circ(\sim 4\%)$ and $\theta_g=157.5^\circ(\sim 6\%)$. This shows consistency of results obtained, indicating that the number of gap elements to model discontinuity does affect the loss factor values only marginally. An optimum selection of the number of gap elements for the same gap size gives better results. The direction of the load with respect to orientation of the gap axis has a greater effect on $(\eta_{22})_t$ and on the percentage increase in $(\eta_{22})_t$. If the orientation of the gap axis coincides with the load vector, there is no effect of slip at the interface on $(\eta_{22})_t$, and $(\eta_{22})_t=(\eta_{22})_{wf}$.

Variation of energy dissipation in transverse shear loading from single- and three-gap element models corresponding to the orientation of the gap axis is plotted in Fig. 13(b). Here also it can be seen that variation of D_i for both single- and three-gap element models are closely related. It may be noted that the use of three-gap elements is primarily to test its adequacy over the single-gap element. Figs. 14(a) and (b) show the variation of $(\eta_{23})_t$ and the percentage increase in $(\eta_{23})_t$ as a function of θ_g, respectively. Thus, a close relationship is observed for $(\eta_{23})_t$ in both the models with a maximum at $\theta_g=135^\circ$. The total loss factor is somewhat higher in case of the three-gap

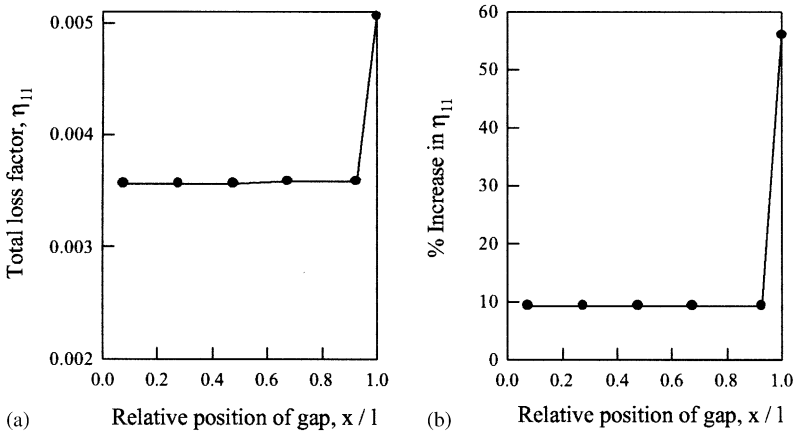

Fig. 16. Effect of location of gap on (a) total η_{11} and (b) percentage increase in total η_{11} (FEM model: longitudinal loading; no. of gap elements = 1; gap size = 23.76 μm; $V_f = 0.4$).

element model as compared to the single-gap element model. The percentage increase in $(\eta_{23})_t$ at $\theta_g = 135^\circ$ is 34.84 (single-gap model) and 40.8 (three-gap element) for the two type of models.

Figs. 15(a) and (b) show the effect of location of the gap along the axis at the interface on $(\eta_{12})_t$ and the percentage increase in $(\eta_{12})_t$. It can be seen that $(\eta_{12})_t$ is almost independent of the relative position of the gap element (x/l) along the fiber length so far as the discontinuity is within the structure $(0 < x/l < 1)$. However, for the discontinuity starting at the edge, i.e., $x/l = 1$, the value of $(\eta_{12})_t$ increases slightly to 1.6×10^{-2}. Similarly, the percentage increase in $(\eta_{12})_t$ for the discontinuity of the same size within the composite, is constant and independent of the relative position of the gap element up to $0.075 \leqslant x/l \leqslant 0.925$. However, for a discontinuity at the edge, i.e., $x/l = 1$, there is a sudden rise in the percentage increase in $(\eta_{12})_t$, of the order of 6.25. This indicates that the effect of debonding or discontinuity at the interface on $(\eta_{12})_t$ is more predominant at the edges. When the damage is away from the edges along the fiber matrix, $(\eta_{12})_t \cong \eta_{12}$ of the pristine material.

Figs. 16(a) and (b) show variation of $(\eta_{11})_t$ and percentage increase in $(\eta_{11})_t$ with the relative position of the gap along the fiber–matrix interface. It can be observed that there is an increase in $(\eta_{11})_t$ in reference to pristine material due to slip at the fiber–matrix interface for the same gap size. However, it is independent of x/l for $0 < x/l < 1$, when the debonding is within the composite. The total loss factor $(\eta_{11})_t$ increases sharply to 5.088×10^{-3} for debonding starting from the edge. Similarly, the percentage increase in $(\eta_{11})_t$ is fairly constant ($\sim 9.4\%$) for $0.075 \leqslant x/l \leqslant 0.925$, whereas at the edge (x/l), it jumps to 56%. Thus, the sensitivity of longitudinal loading on (η_{11}) and the percentage increase in (η_{11}) is indicated through these results.

5. Conclusions

An integrated FEM/Strain energy approach has been worked out to predict loss factors (η_{11}, η_{22}, η_{23}, and η_{12}) for two-phase, three-phase composites with damage (interfacial discontinuity). The following conclusions have been made.

5.1. Two-phase composites

Comparison of damping predictions for two-phase (fiber–matrix) composites are made based on several models and has shown that the finite element/strain energy model based damping results presented here are best for a single representative volume element. Thus, the loss factors are higher for all loading conditions due to the reason that only the actual state of stress is accounted for. There is better correlation of the loss factor predictions made by Eshelby's method, and the Hashin's model, and the Halpin–Tsai and Tsai model. The only exception is the case of the longitudinal loss factor (η_{11}), where deviation is observed in the prediction based on Eshelby's method. The other methods give better results.

Loss factors predicted through the unified micromechanics approach do not compare well with other methods. Consideration of variable stress (in the FEM method) and the additional effect of fiber-to-fiber interaction (in Eshelby's method) render results from these theories rather more accurate.

5.2. Three-phase composites

Damping coefficients for fiber-reinforced composites with hard and soft interphases in longitudinal, transverse, longitudinal and transverse shear loading conditions predicted using the FEM/Strain energy approach employing both the 2D and 3D FEM models provide the understanding as to how damping is related to the modulus and the volume fraction of the interphase. The results provide an insight into the interplay and relative contributions of the three constituents, i.e., the fiber, matrix and interphase, to various damping loss factors. The change in properties of fiber, matrix and interphase will lead to a change in the magnitude of effectiveness of the interphase, but the manner in which the interphase would affect the various loss factors depends predominately upon whether the hard or soft interphase is chosen. Loss factor of fiber-reinforced composites can be improved to a great extent by incorporating highly damped interphases.

5.3. Effect of interface damage

The damage in composite is modelled as a discontinuity at the fiber–matrix interface (debonding) by a 2-D gap element using the finite element method to predict transverse, transverse shear, longitudinal and longitudinal shear loss factors. It is observed that the damping is sensitive to damage and its orientation with respect to the loading directions. The transverse loss factor is maximum when the orientation of discontinuity (angle of orientation of gap) is 45° or 157.5° whereas the transverse shear loss factor has a maximum value for 135° gap orientation. Both longitudinal and shear loss moduli are independent of the location of the discontinuity along the axis of a fiber as far as it is within the composite. The percentage increase in damping is appreciable if the discontinuity is at the edge (approximately 50% for longitudinal load and 6% for longitudinal shear).

Appendix A. Nomenclature

η_{11}, η_{22}, η_{12} and η_{23}	loss factors in longitudinal, transverse, longitudinal and transverse shear, resp.
η_c	loss factor of composite
η_{wf}	loss factor without the consideration of friction at the interface
η_{total}	total loss factor of the composite
W_f, W_i, W_m and W_c	strain energy in fiber, interphase, matrix and composite, resp.
W_{id}	total strain energy with interfacial discontinuity
σ, ε	stress and strain
F_t and F_n	tangential normal forces, resp.
μ	coefficient of friction
F_i	applied force
F_0	force amplitude of applied force
d_s	relative displacement between the nodes of the friction element
D	energy dissipated at the fiber–matrix interface
D_{id}	energy dissipation due to individual discontinuity at interface
T_i	total thickness of the interphase
V_f, V_i and V_m	volume fraction of fiber, interphase and matrix, resp.
GW	gap width
θ_{gs}	gap size
θ_g	gap orientation
N_f and N_m	number of fiber elements in fiber and matrix, resp.
N_g	friction or gap element number
x	location of gap element along the fiber axis
l	length of the model along the fiber axis

References

[1] P. Zioniev, Y.N. Ermakov, Energy Dissipation in Composite Materials, Technomic Publication, Lancaster, PA, 1994.
[2] R.F. Gibson, S.J. Hwang, H. Kwak, Micromechanical modelling of damping in composites including interphase effects, Proceedings of 36th International SAMPE Symposium, Society for the Advancement of Material and Process Engineering, Covina, Vol. 1, 1991, pp. 592–606.
[3] D.J. Nelson, J.W. Hancock, Interfacial slip and damping in fiber-reinforced composites, Journal of Material Science 13 (1978) 2429–2440.
[4] J.M. Kenny, M. Marchetti, Elasto-plastic behavior of thermoplastic composite laminates under cyclic loading, Composite Structures 32 (1995) 375–382.
[5] S. Chang, C.W. Bert, Analysis of damping for filamentary composite materials, Proceedings of Sixth St. Louis Symposium, American Society of Metals, 1973, pp. 51–62.
[6] L.B. Crema, A. Castellani, U. Drago, Damping characteristics of fabric and laminated kevlar composites, Composites 20 (6) (1989) 593–596.
[7] D.A. Saravanos, C.C. Chamis, Unified micromechanics of damping for unidirectional and off axis fiber composites, Journal of Composite Technology and Research 12 (1990) 31–40.

[8] D.A. Saravanos, C.C. Chamis, An integrated methodology for optimizing the passive damping of composite structures, Polymer Composites 11 (6) (1990) 328–336.
[9] M. Kaliske, H. Rther, Damping characterization of unidirectional fiber-reinforced composites, Composite Engineering 5 (5) (1995) 551–567.
[10] R. Chandra, S.P. Singh, K. Gupta, FEM modelling for damping evaluation of fiber-reinforced composites, Proceedings of National Symposium on Dynamics, NASDYN 98, Indian Institute of Technology, Madras, India, 1998, pp. 109–114.
[11] R. Chandra, S.P. Singh, K. Gupta, Comparative study of damping models for fiber- reinforced composites, Proceedings of 11th ISME Conference on Mechanical Engineering, Indian Institute of Technology, Delhi, India, 1999, pp. 489–495.
[12] S.K. Chaturvedi, G.Y. Tzeng, Micromehanical modelling of material damping in discontinuous fiber three-phase polymer composites, Composite Engineering 1 (1) (1991) 49–60.
[13] J. Vantomme, A parametric study of material damping in fiber-reinforced plastics, Composites 26 (1995) 147–153.
[14] I.C. Finegan, R.F. Gibson, Improvement of damping at micromechanical level in polymer composite materials under transverse loading by the use of special fibre coatings, Journal of Vibrations and Acoustics 120 (1998) 623–627.
[15] R. Chandra, Some Micromechanical Studies on Damping in Fiber-Reinforced Composites, Ph.D Thesis, Department of Mechanical Engineering, Indian Institute of Technology, Delhi, India, 1999.
[16] R. Chandra, S.P. Singh, K. Gupta, Damping studies in fiber-reinforced composites—a review, Composite Structures 46 (1) (1999) 41–51.
[17] R. Chandra, A.K. Mallik, R. Praphakaran, Damping as a measure of damage in composites, Journal of Technical Council of ASCE (American Society of Civil Engineers) 108 (1982) 106–111.
[18] J.M. Curtis, D.R. Moore, Fatigue testing of multiangle laminates of CF/PEEK, Composites 19 (1988) 446–455.
[19] E.E. Ungar, E.M. Kerwin Jr., Loss factor of viscoelastic systems in terms of energy concepts, Journal of Acoustical Society of America 34 (1962) 954–958.
[20] Z. Hashin, Analysis of properties of fiber composites with anisotropic heterogeneous materials, Journal of Applied Mechanics 46 (1979) 543–550.
[21] Y.H. Zhao, G.J. Weng, Effective elastic moduli of ribbon-reinforced composites, Transactions of American Society of Mechanical Engineers 57 (1990) 158–167.
[22] S.W. Tsai, Structural behavior of composites materials, NSA-CR-71, July 1964.
[23] J.C. Haplin, S.W. Tsai, Effect of environmental factors on composite materials, AFML-TR, 67-423, June 1969.
[24] JD. Eshelby, The determination of the elastic field of an elliptical inclusion and related problems, Proceedings of the Royal Society, London, 1957, pp. 376–396.
[25] R. Chandra, S.P. Singh, K. Gupta, Micromechanical damping models for fiber-reinforced composites: a comparative study, Composites Part A: Applied Science and Manufacturing 33 (2002) 787–796.
[26] R. Chandra, S.P. Singh, K. Gupta, Studies on prediction of damping in three-phase fiber-reinforced composites: a FEM approach, Defence Science Journal, in press.
[27] V. Tvergaard, Effect of fiber debonding in whisker reinforced metal, Material Science Engineering A 125 (1990) 203–213.